Received: Added at production | Revised: Added at production | Accepted: Added at production

DOI: xxx/xxxx

ORIGINAL ARTICLE

Performance Study of High-Speed Homopolar Inductor Alternator

Vijayasree G.*[1,2] | Mini V. P.[1,2] | Ushakumari S.[1,2]

[1]Department of Electrical Engineering, College of Engineering Trivandrum, Thiruvananthapuram, Kerala, India.
[2]APJ Abdul Kalam Technological University, Thiruvananthapuram, Kerala, India.

Correspondence
*Vijayasree G., Department of Electrical Engineering, College of Engineering Trivandrum, Thiruvanathapuram, Kerala, India. Email: vijayasree@cet.ac.in

Abstract

Recently hydraulic and mechanical-based aircraft systems are replaced by electrical-based 'on board aircraft systems' because of their various advantages like less volume and weight, and reliability. So electrical power system architecture needs to be modified. In spacecraft, a major volume is utilised for the electrical subsystem. The main requirements of the electrical power system of spacecraft are better reliability, less volume and weight, and improved power efficiency. Separate power-generating sources are used for propulsion and various auxiliary systems. Solar-based generation, nuclear-based generation, and fuel cells are some electrical energy sources used in aircraft. More reliable power generation techniques are required for long-duration space missions. The multiphase alternator is a better choice for reliable power generation. Another constraining factor for space power systems is volume and weight because of less space availability in the aircraft. Considering these constraining factors very high power density alternators are suitable for space power systems. Hence, High-Speed Homo Polar Inductor Alternator (HSHIA) is the most suitable candidate. High-speed operation up to 1 lakh RPM is possible with this machine due to its better power density and the special structure of the rotor. This machine already finds application in pulse charging as well as for energy storage by NASA and certain defense organizations. For studying its suitability for auxiliary power generation, a performance analysis is to be carried out. In HSHIA the performance is classified into three levels such as magnetic, electrical, and thermal. This paper presents the electrical performance analysis of HSHIA with different load conditions using the 3 -D Finite Element Method.

KEYWORDS:
performance analysis, power density,energy storage,virtual modeling

1 | INTRODUCTION

High-speed homopolar inductor alternator finds application in flywheel energy storage systems, capacitor charging systems, and some other specific applications in aerospace vehicles. HSHIA has a single piece of iron as a rotor and contains no windings. This enables operating the machine at a very high-speed. This machine is operated as a homopolar pulse generator for the capacitor charging system, otherwise, a complex circuit is required for this purpose. The electrical performance analysis of these machines is required to study the possibility of the application of these machines for general power systems inside space vehicles. This paper discusses the electrical

performance analysis of the HSHIA with different load conditions. As the machine structure is complex, the performance analysis is carried out using 3D model virtually developed in Finite Element Method. For this analysis, a detailed literature review has been carried out. The structure with design and virtual development is presented in [1].G.C.Jain. Design and optimization of HIA is presented by Qian Wang Chengjun Liu, and Jibin Zou, H.[2] and the behavior of Homopolar Inductor MAchine(HIM) is predicted with the help of analysis of the 2D model [3]. Armature reaction has a significant effect on inductance and resistive loads [4]. The influence of the width, depth, and the number of slots on the eddy current loss is investigated in the paper by Jiangtao Yang, et. al[5]. It is shown that the circumferential slits have better performance than the axial slits to reduce the eddy current loss. The various inductances and saturation effects of inductances are studied in[6]. Electromagnetic performance analysis of homopolar inductor machine through the nonlinear magnetic equivalent circuit and airgap permeance function is explained by Jiangtao Yang, et. al[7]. A new topology with an outer rotor structure is proposed in[8]by Jiangtao Yang, et. alfor improving the power density. A comparison of the fault tolerant operation of three phase and different winding configurations of dual three phase induction motors is presented with experimental data by Luigi Alberti, and Nicola Bianchi [9]. The equivalent magnetic model of reactive homopolar synchronous machine with stator excitation is presented by Sorin Ioan Deaconu et.al[10]. Operation of the six-phase induction machine presented by Che ,Hang Seng.et .al[11].The similarity in design and structure of the stator of HIM and synchronous machine is explained by Ye. Cayong et. al[12]. Decoupled vector control of dual three phase PMSM machines is introduced by Kartunen Jussy et.al [13]. Kexun Yu et.al, describe the eddy current loss of unlaminated structure of rotor used in homopolar machines used for pulse supply applications with nonlinear load[14]. Modeling methods of asymmetrical six-phase machines are studied by Zabaleta et. al [15]

From the study of literature carried out, it is seen that a detailed performance analysis of HSHIA has not been carried out. For the applications mentioned, a detailed analysis of HSHIA based on requirements such as power density, efficiency, and losses is to be done. This paper proposes a detailed performance analysis of HSHIA.

This paper is organized into five sections, after the introduction second part is discussed the structure and principle of operation of HSHIA. Its design and virtual development are explained in section 3,and section 4 deals with the performance analysis. The result and discussion and conclusion are presented in sections 5 and 6 respectively.

2 | STRUCTURE AND THE PRINCIPLE OF OPERATION

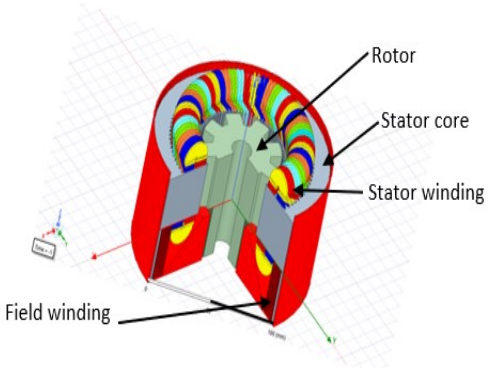

Figure 1 Structure of HSHIA

The structure of HSHIA is shown in Fig.1. The main parts include the stator, rotor, stator winding, and field winding. The rotor of HSHIA is a toothed wheel with slots and teeth displaced by 180-degree electrical. The number of teeth is equal to the designed number of poles. The rotor contains no winding and field winding is provided surrounding the stator core. When field winding is energized, emf is induced across stator conductors due to the variable reluctance of air gap.

As shown in Fig.1,this machine has stator core made up of steel laminations. The concentrated field winding encircles a rotor structure. Distributed six-phase winding is provided in the axial slots provided on the inner part of the stator core. The rotor is constructed with unlaminated steel and it has an equal number of projected poles on either side which are differed by 180 electrical degrees. An outer cover is provided which acts as a path for magnetizing flux. When field winding is excited with a constant current, the homopolar magnetic flux is formed, and the corresponding air gap flux density distributions are shown in Fig.2.[12]

In HSHIA, the magnetomotive force (MMF) of opposite polarity is generated on left and right air gaps. It is given as

$$F_{Right} = -F_{Left} = \frac{N_F I_f}{2} \tag{1}$$

Where F_{Right} and F_{Left} are MMF created by the field winding acted upon the left and right side of the air gap. Flux created in the air gap shown in Fig. 2. It can be seen that direction of magnetising flux on the air gap on either side is opposite to each other due to 180 degrees offset between the poles on both ends of the rotor. The flux through per turn of of the stator

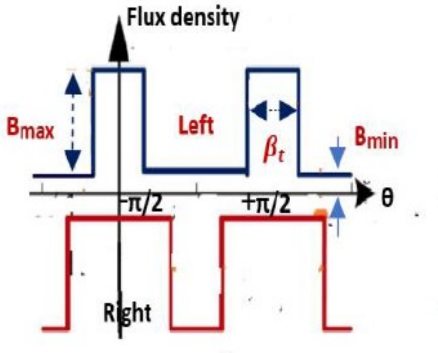

Figure 2 Flux density distribution in HSHIA

winding is obtained by

$$\phi_{winding} = \int (B_L + B_R) r l d_\theta \tag{2}$$

Where, r is the radius of stator conductor and l is the length of one turn of stator coil. Generated -EMF per phase of HSHIA is expressed as

$$E_{phase} = N \frac{d\lambda_{winding}}{d_t} \tag{3}$$

where $\lambda_{winding}$ indicates the flux linkage in the winding on

3 | DESIGN AND VIRTUAL DEVELOPMENT OF HSHIA

The design of HSHIA is started with mathematical equations (Jain, 2020). The important equations are:

Table 1 Specifications of HSHIA

Parameter	Specification
Capacity	2.5kVA
Speed	30000rpm
Frequency	4000Hz
No. pf phases	6

$$Q = C_o D^2 L n_s \tag{4}$$

Where C_o is the output coefficient D and L are stator bore diameter and stator core length respectively. n_s represents speed in rps.

$$T_{ph} = \frac{E_{phase} A}{4.44 f k_w \phi} \tag{5}$$

For design, a 2.5kVA High-Speed Homopolar Inductor Alternator is considered, and Table 1 shows its detailed specifications. For design purposes, certain assumptions are considered. The specific magnetic loading is selected to a low value to minimize the iron losses. The lower value of specific electric loading reduces the copper loss and improves efficiency. A smaller value of the winding factor is selected to reduce the size of the machine. Peripheral speed is limited to a low value to reduce mechanical stress and improve the rotor integrity. Assumed values are given in Table 2, and Table 3 shows the significant dimensions obtained from mathematical design. These dimensions are used to develop a virtual model of HSHIA. In the conventional design of electrical

Table 2 Assumptions

Parameter	Assumptions
Magnetic loading Bav	0.54
Electric loading ac	9000
Winding factor	0.845

Table 3 Assumptions

Parameter	Value
Bore diameter	57.29mm
Length of Armature	33.7mm
Pole pitch	11.24mm
No. of slots	96 Nos.
No. of conductors	800Nos.
Width of slot	5.54mm
Height of slot	16.63mm
Outer diameter	101.58mm
Diameter of Rotor	56.69mm
Area of cross-section of stator conductor	1.9828mm

machines, the cognitive equations according to lumped parameters of the linear magnetic circuit are considered. The slots of the machine are assumed to be rectangular in shape, and the core is working under saturation. Due to the Complex geometry and non-linear material used in HSHIA,these assumptions are invalid. Because of the non-uniform air gap present in the structure of HSHIA, the mathematical formulation for specifying the boundary is complex, and the selection of material parameters is tedious. The finite element method is most suitable for the design and modeling of the HSHIA with

a non-uniform air gap and non-linear material with complex geometry. Fig.3 shows the cross section of the virtual model of HSHIA. The design of HSHIA using FEM helps to determine the significant parameters such as flux linkages, generated EMF, and losses. In FEA, the performance of HSHIA is analysed accurately without any assumptions. ANSYS Maxwell is a high-level interdependent simulation platform based on FEM to solve three-dimensional (3D) electric, magnetostatic, eddy current, and transient problems. In this work, electrical transient solver is used for analysis.

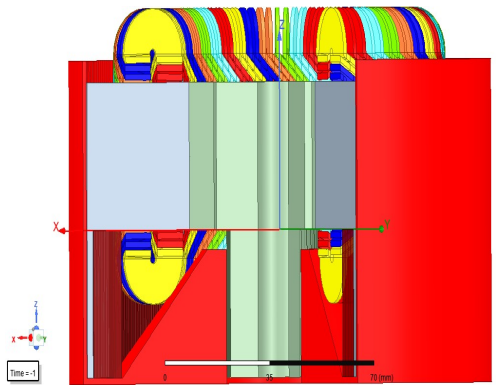

Figure 3 Cross Sectional view of virtual model

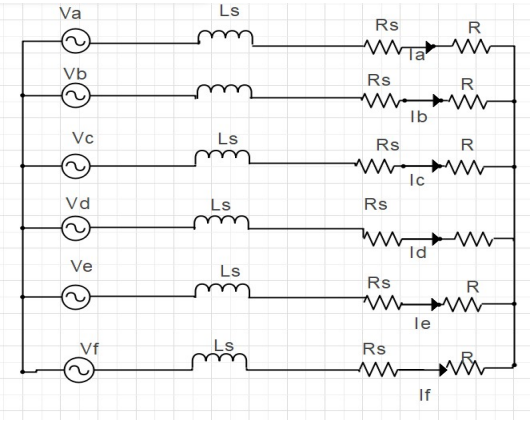

Figure 4 Electrical circuit of six-phase HSHIA

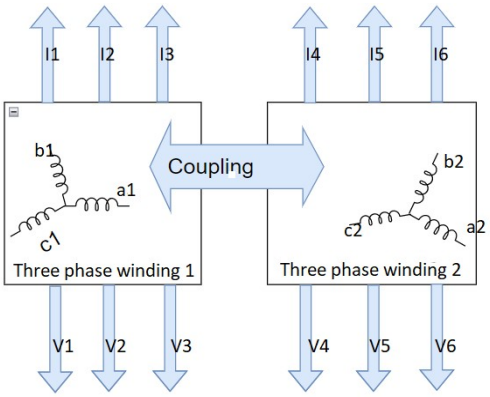

Figure 5 Dual three phase winding

4 | ELECTRICAL ANALYSIS

The outcome of electrical analysis includes generated voltage, current and electrical parameters,and losses. For electrical performance analysis, a six-phase 30000rpm 4kHz 2.5kVA High-Speed Homopolar inductor alternator is considered and its electrical circuit is shown in Fig 4.

In this work, a six-phase system is realised by two three phase subsystems. The dual three-phase machine is supplied by two three-phase subsystems with a displacement of 30 electrical degrees with respect to the other[13]. This approach replaces both three-phase winding sets with equivalent d-q windings in two pairs of d-q equations and Fig.5 shows the dual three-phase winding system[13]

$$V_{q1} = r_1 i_{q1} + \omega_e \psi_{d1} + p\psi_{q1} \quad (6)$$

$$V_{d1} = r_1 i_{d1} + \omega_e \psi_{q1} + p\psi_{d1} \quad (7)$$

$$V_{q2} = r_2 i_{q2} + \omega_e \psi_{d2} + p\psi_{q2} \quad (8)$$

$$V_{d2} = r_2 i_{d2} + \omega_e \psi_{q2} + p\psi_{d2} \quad (9)$$

The matrix for transformation [C] for a dual three phase machine with a phase shift of 30 degrees between two three phases is given.

$$\begin{bmatrix} 1 & -1/2 & -1/2 & 0 & 0 & 0 \\ 0 & -\sqrt{3}/2 & -\sqrt{3}/2 & 0 & 0 & 0 \\ 1/2 & 1/2 & 1/2 & 0 & 0 & 0 \\ 0 & 0 & 0 & -\sqrt{3}/2 & -\sqrt{3}/2 & 0 \\ 0 & 0 & 0 & 1/2 & 1/2 & -1 \\ 0 & 0 & 0 & 1/2 & 1/2 & 1/2 \end{bmatrix}$$

In each row, the coefficients represent two separate three phase transformations, affect only the phase variables of one of the three phase systems. The first three rows represent α_1,β_1, and zero sequence components for the first three-phase system and the next three rows represent α_2, β_2, and zero sequence components for the second three-phase system. With this, the two three-phase systems are addressed separately[15].

As a result, it can be confirmed with the application of the "double d-q transformation", both the three phase systems are considered separately. This is equivalent to two separate three-phase machines with 30- degree phase shifted windings. The physical consequence of this approach is that it produces

two parallel three-dimensional subspaces to which the details of each of the three-phase system are mapped. Direct and quadrature axis equivalent circuit for six phase HSHIA is shown in Fig.6.

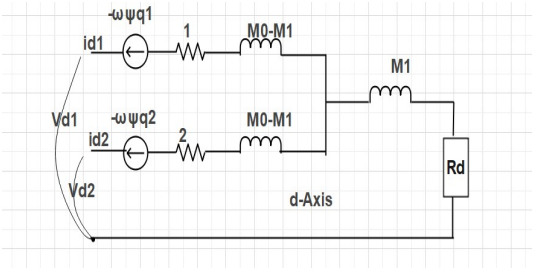

Figure 6 d-q transformed circuit of six phase HSHIA

$$I = I_d + jI_q \tag{10}$$

$$E_{af} = V + Ir_a + jIX_q + j(X_d - X_q)I_d \tag{11}$$

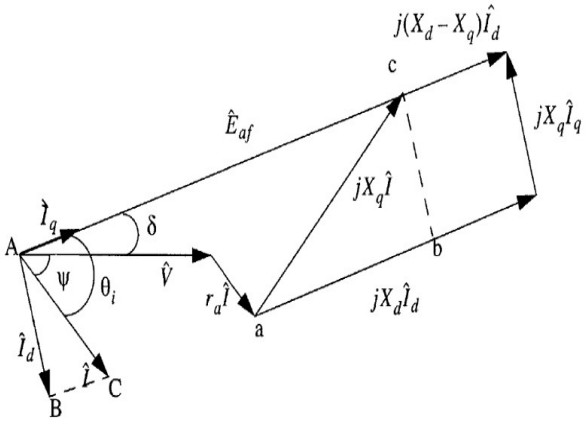

Figure 7 Phasordiagram of HSHIA

The phasor diagram of the HSHIA is given in Fig.7 where E_{af} is the generated emf,V is the terminal voltage, I is the stator current per phase $I_d = Icos\theta$ is the direct-axis current, $I_q = Isin\theta$ is the quadrature-axis current, r_a is the armature resistance, X_d is the direct-axis reactance, and X_q is the quadrature-axis reactance. From the phasor diagram it can be seen that the generated EMF is the sum of terminal voltage, resistive drop, and drop in direct and quadrature reactance. Angle ψ is the power factor angle, θ is the internal power angle and δ is the load angle[14]

5 | RESULTS AND DISSCUSSION

For doing performance analysis the specified HSHIA is considered. Different steps in the analysis process in MAXWELL 3D are explained in the process flow diagram of Fig.8.

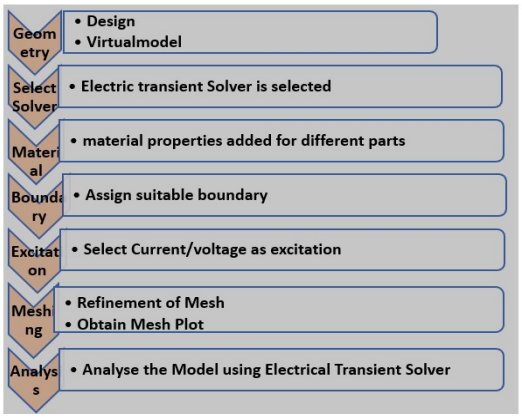

Figure 8 Process Diagram for Electrical Analysis

3-dimensional geometry of HSHIA is developed in MAXWELL 3D using the data obtained from the design which is shown in Fig.9. Virtual model of the rotor structure is shown in Fig. 10

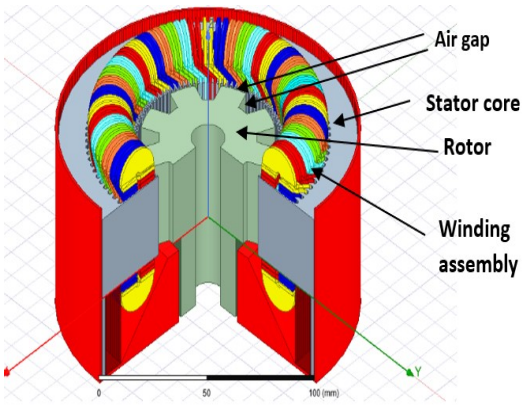

Figure 9 virtual model of HSHIA

For performance analysis, materials are selected for every part of the machine and material properties are added. The properties of the material include relative permittivity and bulk conductivity. Relative permittivity has an effect on the electric field in dielectrics. Conductivity defines whether the material is an insulator or a conductor. These two are selected as 'simple' for the analysis of HSHIA.

The material used to manufacture stator conductors and field

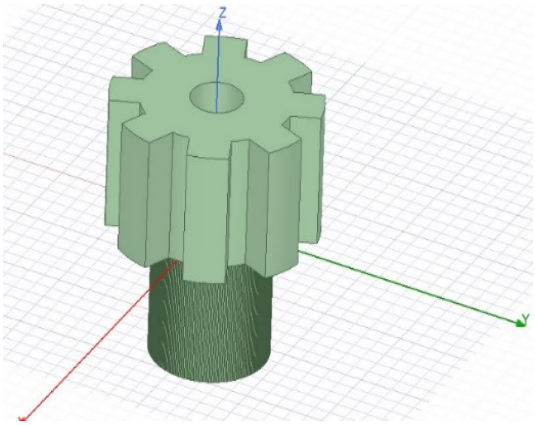

Figure 10 virtual model of rotor of HSHIA

coils is copper. The silicon steel *steel*_1008 is used to develop the stator and rotor core of the HSHIA. Table 4.0 gives the Element components and their percentage in *steel*_1008. Details of materials used to develop the different parts of HSHIA are given in Table 5.

Table 4 Components of steel_1008

Element	Content%
Iron	99.3-99.7
Manganese	0.30-0.50
Carbon	0.10
Sulpher	0.050
Phosphorous	0.040

Table 5 Materials used in HSHIA

Sl. No	Parts	Materials
1	Stator core	Laminated Steel_1008
2	Stator Conductor	Copper
3	Rotor	Solid Steel_1008

Electric Transient Solver is used for electrical performance analysis. Electric transient solver calculates time-varying electric fields within lossy conductors and insulators. Time-varying electric field may be created by transient potential, distributed charge, or current input. Adaptive mesh refinement is not provided in transient solvers, so deliberate meshing is needed. Boundary conditions are to be assigned for defining the nature of the field at the boundary of the geometry and on the edges of the region. There are different boundary conditions that can be added in the electrical transient solver as default boundary, insulating boundary, symmetry boundary, or Master/Slave boundary. Here, default or no boundary is assigned which has two types of treatments on boundaries-natural boundary and Neumann boundary. The natural boundary is assigned to the interface between parts of a different material. The distribution of surface charge per unit area at the boundary area influences the normal component of electric field density across the boundary. Neumann boundary is assigned for exterior boundaries of the geometry and an electric field is tangential to the boundary. A constant current of 10 A is assigned as the excitation. In solution set up stop time and step size are assigned.

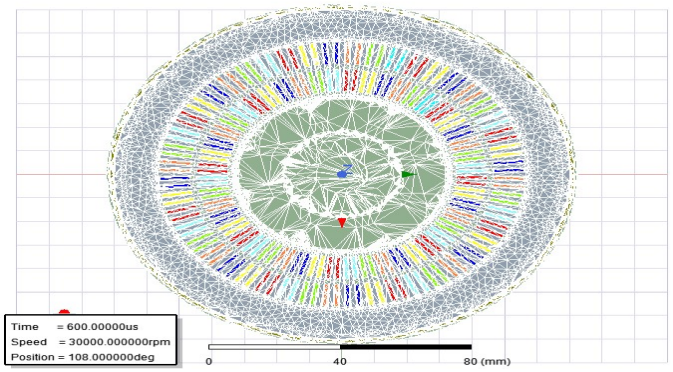

Figure 11 Mesh diagram of full section of HSHIA

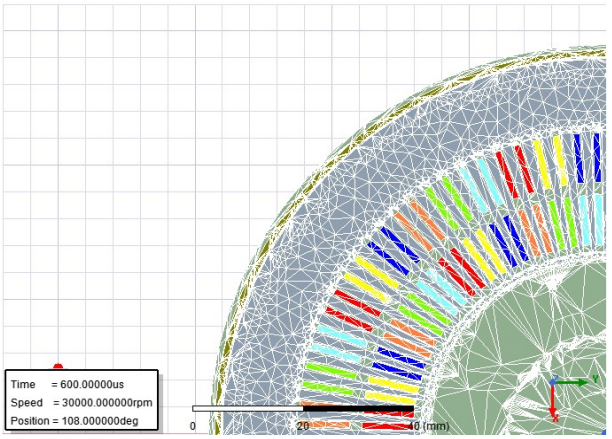

Figure 12 Mesh diagram of one fourth section of HSHIA

The geometry of the machine is discretized into finite elements with tetrahedral shapes. As a result of this,the number of equations as much as the number of finite elements is

obtained. The assembly of all these elements is known as mesh and the processing is known as meshing or discretization. Mesh resolution is an important factor in deciding the accuracy of the computed solution. The automatic refinement of mesh is done in certain solvers of MAXWELL, which is called adaptive mesh refinement and is not provided with transient solvers. When the solution process is initiated, an initial mesh is created by the software automatically for doing field calculations without any instruction. As transient solvers do not have the provision for refining the initial mesh, a suitable mesh operation should be specified or should link with an adaptive mesh refinement from a static solver. The mesh operations offered by MAXWELL 3D are 'on selection/length based','on selection /skin depth based', 'inside Selection/ Length Based', 'surface approximation', 'model resolution', and 'cylindrical gap treatment'. Here 'on selection /length based' option is selected for this analysis. This option refines the mesh by controlling the maximum element size on the boundary of assigned objects. When the analysis process begins mesh operations are applied to the initial mesh automatically. Before starting the solution process the quality of mesh and number of elements can be verified by inspecting mesh statistics and also by visual inspection of mesh plots. A mesh plot of the geometry or various parts of geometry is obtained from MAXWELL 3D which can be used to verify the validity of each part. The mesh plots of full section and one-fourth section of HSHIA obtained are shown in Fig.11 andFig 12resprectively[16].

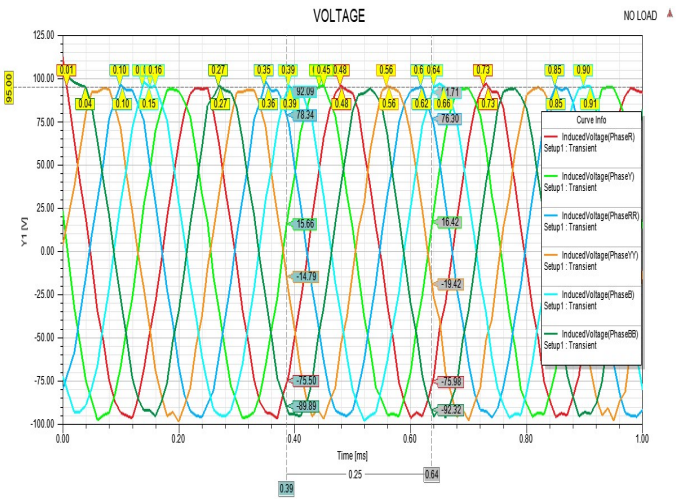

Figure 13 Generated Voltage of HSHIA at no-load

Generated emf obtained from the six-phase developed HSHIA is shown in Fig.13,rotating at a speed of 30000 rpm for an excitation current of 10 amp under no load condition.

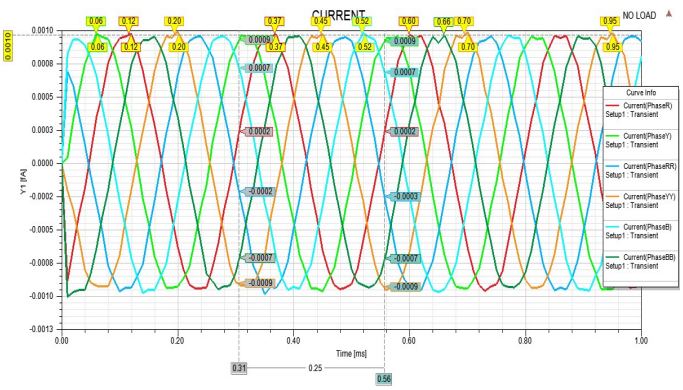

Figure 14 No-load current of HSHIA

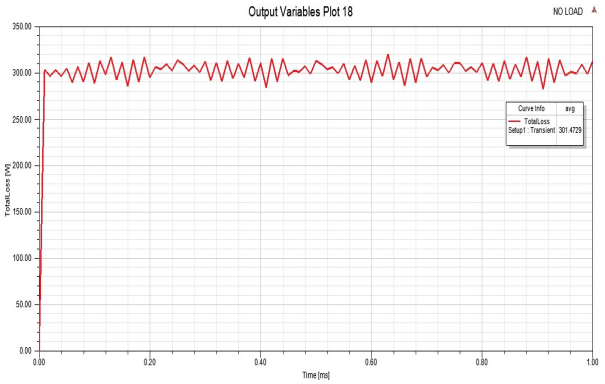

Figure 15 Total loss at no load condition

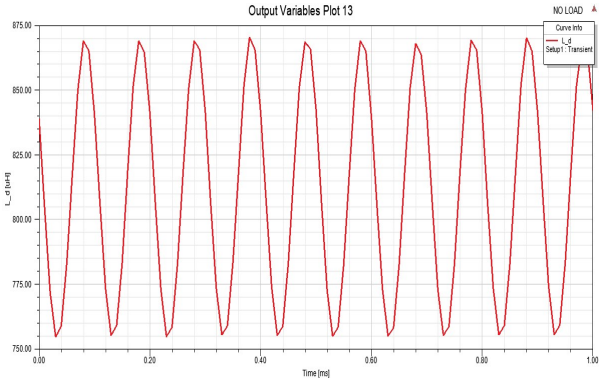

Figure 16 Direct axis Inductance L_d

The Current response is given in Fig.14. The magnitude of voltage generated is 95V (peak) and a current of 0.001A, and the frequency of generated emf is 4kHz. The total loss obtained at no load condition is 301W and it is shown in Fig.15. d- axis and q- axis components of winding inductance of developed HSHIA are shown in Fig.16 and 17respectively. Six phase current is transformed into d-q component using double d-q Parke's transformation. Efficiency at no load condition is

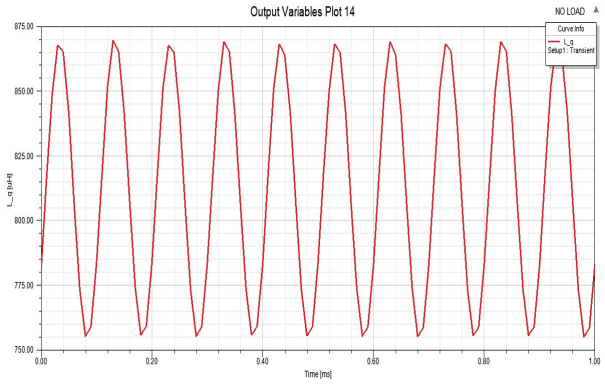

Figure 17 Quadrature axis InductanceL_q

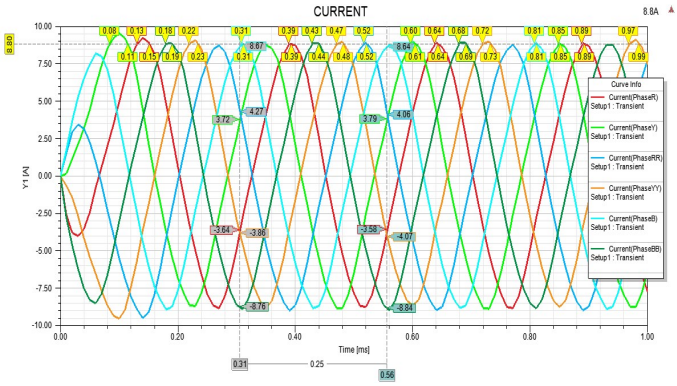

Figure 19 Current at fulload (upf)

found as 87%.

The performance analysis of HSHIA with different load conditions is discussed in the following sub-sections. Fig.18 shows the generated voltage at full load at a power factor unity. From this, it is seen that the magnitude of voltage under full load condition is 66.5 V (peak) and current per phase is 8.8A (peak) and is shown in Fig.19. When the generator is loaded, generated emf is reduced due to skin effect and dc magnetization. The other performance such as flux linkages of six phases, and total loss at full load condition with unity power factor are shown in Fig 20 and 21 respectively. The total loss obtained for full load at upf is 197W and Efficiency at full load condition is 91%.

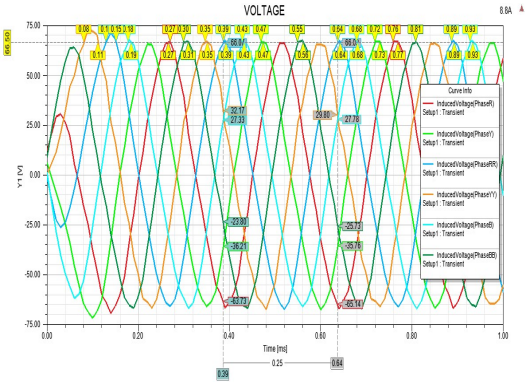

Figure 18 Generated voltage (V) at fulload (upf)

Table 6 Performance Parameters at various load conditions

Load Condition	Generated EMF (peak) V	Current (peak)(A)	Loss (W)
No load	95	0.001	301
¼ Full load	93	2.2	285.8
½ Full load	87.5	4.4	260
Full load upf	65	8.8	197
Full load 0.8 pf lag	43	8.8	165

Table 7 Losses obtained at Different Load condition

Load	Wc(W)	We(W)	Wh(W)	Wcu (W)
No load	300	289	11	0.2832
¼ Full Load	284.8	274.2	9.9	0.35
Half Full load	259	248.5	9.85	0.81
¾ Full load	228.5	218.5	9.43	1.5
Full load (upf)	193	184.7	8.3	2.53
Full load (0.8 pf lag)	162.15	155.59	6.12	2.63

Fig.22 shows the generated voltage at full load at a power factor 0.8 lag. From this, it is seen that the magnitude of voltage under full load condition with RL load is 43 V (peak) and current per phase is (8.8)A peak and is shown in Fig 23. The total loss obtained for full load at 0.8 pf lag is 165W which is shown in Fig.24. Performance parameters of HSHIA at various load conditions are shown in Table 6. Different losses at no load and full load conditions are obtained from the electrical analysis. The eddy current loss of 290W, excess loss of 0.72W, Hysteresis loss of 9.9W, and copper loss of 0.2W. are obtained for no load conditions. The eddy current loss of 185W, excess loss of 0.52w, Hysteresis loss of 8.36W and copper loss of 2.53W. are obtained for full load conditions.

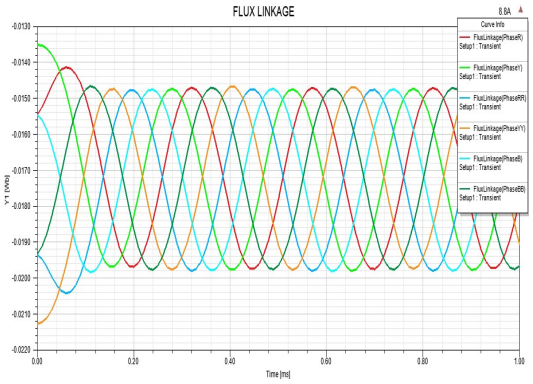

Figure 20 Flux Linages of six phases of HSHIA

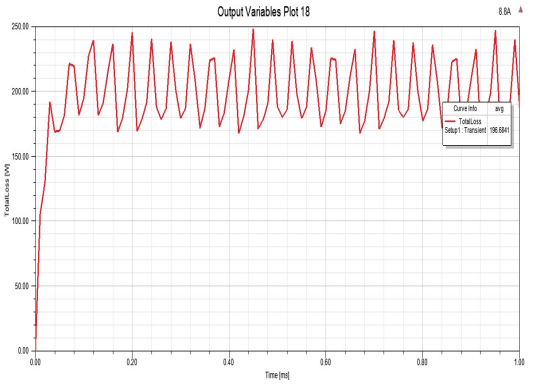

Figure 21 Total Loss of HSHIA at full load

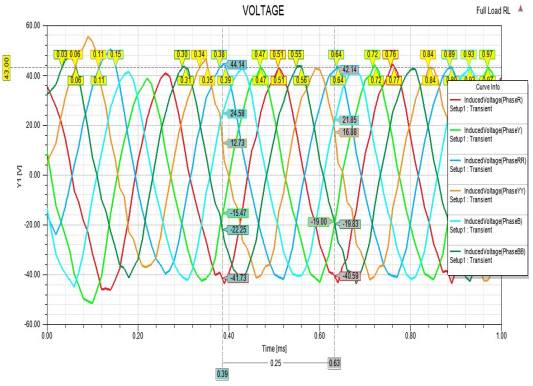

Figure 22 Generated Voltage (V)at fullload (0.8pf lag)

Detailed list of losses obtained with different load condition is given in Table7.

The major part of the loss in HSHIA is the core loss of which eddy current loss has a high value compared to the other losses. Even though the core loss or iron loss is supposed to be constant irrespective of the load conditions, the core loss is reduced considerably from no-load to full load for HSHIA. This is due to the dc magnetization and the armature reaction effect.

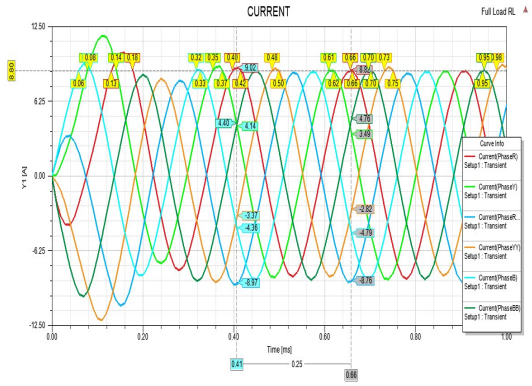

Figure 23 fullload current (A)(0.8pf lag)

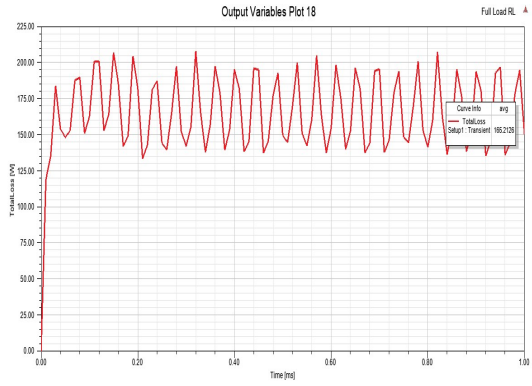

Figure 24 Total Loss at fullload and 0.8pf

6 | CONCLUSION

This paper presents the performance analysis of HSHIA using ANSYS MAXWELL software. A 2.5kVA HSHIA is mathematically designed and virtually developed for performance analysis. The analysis is carried out with a constant current excitation of 10A at different load conditions. From the analysis, the following observations were confirmed. Generated emf and current under no-load and at different load conditions with different power factors were analysed.The loss analysis was carried out. Full load efficiency is high and so this machine is suitable for auxiliary power generation in aerospace power systems. Even though the machine has poor voltage regulation, due to its high reliability and less weight, HSHIA is suitable for aerospace systems. This work can be extended to provide efficient control techniques to improve voltage regulation.

ACKNOWLEDGMENTS

The authors express their profound gratitude to the electrical engineering department, College of Engineering Trivandrum(CET) and APJ Abdul Kalam Technological University (KTU) for granting the essential tools for doing research.

STATEMENT AND DECLARATIONS

- funding was received to assist with the preparation of this manuscript.
- The authors have no relevant financial or non-financial interests to disclose.

References

[1] G. C. Jain, "Design Aspects of a Homopolar Inductor-Alternator," in IEEE Transactions on Power Apparatus and Systems, vol. 83, no. 10, pp. 1009-1015, Oct. 1964, doi: 10.1109/TPAS.1964.4765934.

[2] Wang, Qian, et al. "Numerical analysis and design optimization of a homopolar inductor machine used for flywheel energy storage." IEEE Transactions on Plasma Science 41.5 (2013): 1290-1294.

[3] Tsao, Perry, Matthew Senesky, and Seth R. Sanders. "An integrated flywheel energy storage system with homopolar inductor motor/generator and high-frequency drive." IEEE Transactions on Industry Applications 39.6 (2003): 1710-1725.

[4] GLou Zhenxiu, Yu Kexun, Ren Zhangao and Ye Caiyong, "Analysis of homopolar inductor alternator for high reliability high power density applications," 2009 IEEE 6th International Power Electronics and Motion Control Conference, Wuhan, China, 2009, pp. 841-844, doi: 10.1109/IPEMC.2009.5157501.

[5] Fu, Xinghe, et al. "Calculation and analysis of iron loss in homopolar inductor alternator." IEEE transactions on magnetics 48.11 (2012): 3466-3469.

[6] Xin, Qingming, et al. "Inductance mathematic model of homopolar inductor alternator in a novel pulse capacitor charge power supply." 2012 16th International Symposium on Electromagnetic Launch Technology. IEEE, 2012.

[7] Yang, Jiangtao, et al. "Analysis of the electromagnetic performance of homopolar inductor machine through nonlinear magnetic equivalent circuit and air-gap permeance function." IEEE Transactions on Industry Applications 56.1 (2019): 267-276.

[8] Yang, Jiangtao, Caiyong Ye, and Shoudao Huang. "Development and analysis of an outer rotor homopolar inductor machine for flywheel energy storage system." IEEE Transactions on Industrial Electronics 68.8 (2020): 6504-6515.

[9] Alberti, Luigi, and Nicola Bianchi. "Experimental tests of dual three-phase induction motor under faulty operating condition." IEEE Transactions on Industrial Electronics 59.5 (2011): 2041-2048.

[10] Deaconu, Sorin Ioan, et al. "Mathematical model of a reactive homopolar synchronous machine with stator excitation." 2009 13th European Conference on Power Electronics and Applications. IEEE, 2009.

[11] Che, Hang Seng, et al. "Operation of a six-phase induction machine using series-connected machine-side converters." IEEE Transactions on industrial Electronics 61.1 (2013): 164-176.

[12] Ye, Caiyong, et al. "Relationship between homopolar inductor machine and wound-field synchronous machine." IEEE Transactions on Industrial Electronics 67.2 (2019): 919-930.

[13] Karttunen, Jussi, et al. "Decoupled vector control scheme for dual three-phase permanent magnet synchronous machines." IEEE Transactions on Industrial Electronics 61.5 (2013): 2185-2196.

[14] Z. Ren, K. Yu, Q. Xin and Y. Pan, "Performance of Homopolar Inductor Alternator With Diode-Bridge Rectifier and Capacitive Load," in IEEE Transactions on Industrial Electronics, vol. 60, no. 11, pp. 4891-4902, Nov. 2013, doi: 10.1109/TIE.2012.2227908.

[15] Levi, E., M. Zabaleta, and M. Jones. "Modelling Approaches for an Asymmetrical Six-Phase Machine." International Symposium on Industrial Electronics (ISIE). IEEE, 2016.

[16] Hans, Vande Sande. "Modelling and finite element simulation of non-linear and anisotropic quasi-static electromagnetic systems."

□